This article has been accepted for publication in a future issue of this journal, but has not been fully edited. Content may change prior to final publication. Citation information: DOI 10.1109/TSG.2017.2648879, IEEE Transactions on Smart Grid

Fault Characteristics Analysis and Line Protection Design within a Large-Scale Photovoltaic Power Plant

Ke Jia, Chenjie Gu, Zhenwen Xuan, Lun Li and Yaoqi Lin

***Abstract*—Centralized photovoltaic (PV) systems have different fault characteristics from distributed PV systems due to the different system structures and controls. This makes the fault analysis and protection methods used in distribution networks with distributed PV not suitable for a centralized PV power plant. Therefore, a consolidated expression for the fault current within a PV power plant under different controls was calculated considering the fault response of the PV array. Then, supported by the fault current analysis and the field-testing data, the overcurrent relay (OCR) performance was evaluated in the collection system of an 850 MW PV power plant. It reveals that the OCRs at PV side on overhead lines may malfunction. In this case, a new relay scheme was proposed using directional distance elements. In PSCAD/EMTDC, a detailed PV system model was built and verified using the field-testing data. Simulation results indicate that the proposed relay scheme could effectively solve the problems under variant fault scenarios and PV plant output levels.**

***Index Terms*—centralized photovoltaic power plant, distance relay, fault current analysis, overcurrent relay (OCR), relay scheme**

I. Introduction

DUE to the increasing energy crisis and environmental problems, the grid-connected PV generation has grown rapidly [1]. The worldwide solar installation capacity is 59GW (mostly in the power plant form) in 2015 and another 64GW will be installed in 2016 [2]. Within a large-scale PV power plant, PV units are collected via overhead lines and cables. The limited fault current characteristics within the plant challenge the existing protective relays. Once a fault occurs within the plant, the relay's incorrect operation may lead to disconnection of the non-fault sections and the fault may be remained for a relative long time.

Grid codes require PV plants with the fault-ride-through (FRT) ability [3], [4]. For the FRT accomplishment, variant controls in the PV inverter have been investigated. The fault current characteristics of the PV inverter show diversity due to different FRT controls. The maximum fault current allowed through power electronic devices is limited for the device safety. Therefore, it is difficult to estimate the exact fault current and this brings challenges to current based protection designs.

The current controllers under a double synchronous rotating frame (DSRF) [5] are widely used in centralized PV inverters. In this control frame, several FRT controls have been investigated: 1) the control that eliminates the active output power oscillation results in injection of the negative-sequence current and the reactive output power oscillation [6]; 2) the control that suppresses the negative-sequence current causes both the active and the reactive output power oscillations [7]; 3) the control that eliminates both the active and the reactive output power oscillations has the problem of current distortions [8]. The diverse controls lead to variant fault current characteristics and the flexible control is investigated to make a tradeoff between the current quality and the power oscillation [9]. Researches on the fault current calculation of inverter-interface sources took the assumption that the active power supply from dc side keeps constant after a grid-side fault [10]-[12]. Those papers held the view that the slow dc-link voltage control loop provides a constant power reference and the fast response of the PV panel to the grid voltage variation is ignored. In [13] the PV panel characteristic was considered to help enhance the FRT ability but those effects on the fault current were not analyzed.

Relay designs are based on the fault current analyzing. Investigations on the protective relays in consideration of PV penetrations are focused on the distribution level with distributed generations (DGs). The performance of the traditional overcurrent relays (OCRs) is evaluated by considering the unique renewable source features, locations and penetration capacity of DGs [14]-[16]. The original protection coordination is challenged due to the massive renewable sources integration, thus directional OCR was introduced to solve this problem [17], [18]. Directional OCRs with communication capabilities are used to minimize the number of disconnected DGs once faults occur [19]. The protection schemes based on the steady-state fault current calculation from steady-state network equivalent reduction and the current phase angle comparison have been also proposed in [20] and [21], respectively.

The distributed PVs generally use the control in the positive-sequence frame and an unbalanced fault may cause current distortions and harmonics [22]. The centralized PVs have different fault current characteristics from the distributed PVs due to an additional negative-sequence control loop and the unique single-stage topology (without the DC/DC boost circuit). The fault analysis methods and protection principles in distribution networks can hardly be applied within the PV power plant. For the single-stage PV system, the PV panel characteristic should be considered. The output power of the PV panel changes with its interfaced dc-link voltage.

In this paper, in order to comprehensively evaluate the performance of the existing protection design within the PV power plant, a consolidated expression of the fault current, suitable for different inverter controls is calculated and analyzed. The analysis is confirmed using both the fielding testing and simulation results. Based on this, the existing OCRs within the plant are examined and the problem of malfunction is revealed. A distance relay based scheme is proposed to improve the existing OCR and is highly robust to different fault scenarios and output levels of the PV power plant.

The remaining paper is organized as follows. Section II discusses the fault current characteristics within a large PV power plant. In Section III, the performance of the existing OCRs within the PV power plant is evaluated and a distance relay based protection scheme is proposed. In Section IV the field-testing results verify the above analysis and simulation results show that the proposed relay scheme can protect the system effectively. Conclusions are drawn in Section V.

II. Characteristics of Fault Current

A. Overview of the Collection System

One of the collection systems within an 850 MW PV power plant is discussed here. The collection system collects 64 PV units totally, 1 MW for one generation unit, as shown in Fig. 1. Every 4 cables feed into one 35 kV bus and each cable collects 8 PV units. The collection system is connected with the main transformer through 35 kV overhead lines.

B. Control Strategy

The fault characteristics within the collection system are dependent on the control of PV inverters and the fault current analysis is based on the proper representation and modelling of the inverter control system.

The DSRF-based control scheme is widely used in commercial products, since the reference current estimation can be simplified for the decoupling relation between the active and reactive powers [23]. In order to realize the more flexible fault-ride-through (FRT) control, the inner-loop current control uses the regulators under a DSRF, and the outer-loop voltage control regulates the dc-link voltage to realize maximum power point tracking (MPPT) that is used in [24]. In the control system, a synchronous reference frame phase-locked loop (SRF-PLL) is important for grid synchronization and control performances [25]. However, the SRF-PLL might bring unsatisfying results for unbalanced fault conditions [26]. Here, a notch filter (NF), a band-rejection filter with a narrow stop bandwidth, is integrated into the conventional PLL system to eliminate undesired harmonic components, as used in [27]. The detailed control system is presented in Fig. 2.

Considering unbalanced grid voltage conditions, the instantaneous active and reactive power injection from the PV inverter can be expressed as [5]

$$\begin{cases} P = P_0 + P_{c2}\cos(2\omega t) + P_{s2}\sin(2\omega t) \\ Q = Q_0 + Q_{c2}\cos(2\omega t) + Q_{s2}\sin(2\omega t) \end{cases} \tag{1}$$

where P_0 and Q_0 are the average values of the active and reactive output powers, and P_{c2}, P_{s2}, Q_{c2} and Q_{s2} are the power amplitudes of the individual second harmonic components. Using the sequence components of voltages and currents in the DSRF, the above six power amplitudes can be calculated as [5]

$$\begin{bmatrix} P_0 \\ P_{c2} \\ P_{s2} \\ Q_0 \\ Q_{c2} \\ Q_{s2} \end{bmatrix} = \frac{3}{2} \begin{bmatrix} e_d^+ & e_q^+ & e_d^- & e_q^- \\ e_d^- & e_q^- & e_d^+ & e_q^+ \\ e_q^- & -e_d^- & -e_q^+ & e_d^+ \\ e_q^+ & -e_d^+ & e_q^- & -e_d^- \\ e_q^- & -e_d^- & e_q^+ & -e_d^+ \\ -e_d^- & -e_q^- & e_d^+ & e_q^+ \end{bmatrix} \begin{bmatrix} i_d^+ \\ i_q^+ \\ i_d^- \\ i_q^- \end{bmatrix} \tag{2}$$

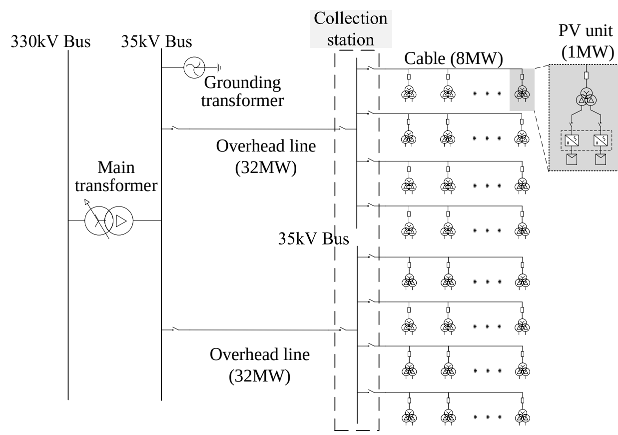

Fig. 1. A collection system within a large-scale PV plant.

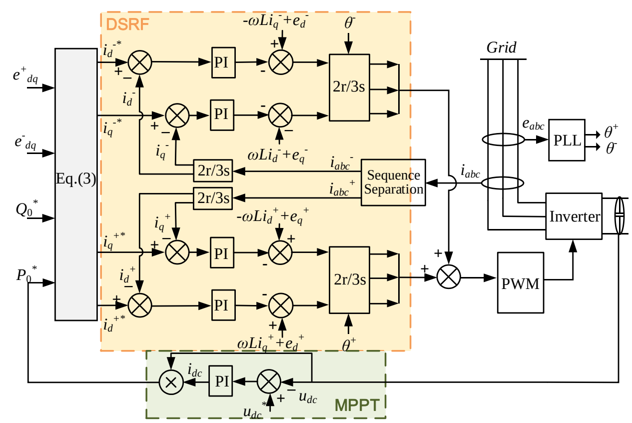

Fig. 2. The block diagram of the inverter control system.

The coefficient matrix in (2) is not reversible and the four current freedoms cannot control the six power amplitudes at the same time. It is only possible to set the four of them and two variables are set to zero. In view of practical applications, the negative-sequence currents are usually set to zero [7]. With a factor K denoting the used control strategy, the current references under different controls can be rearranged and calculated as [28]

$$\begin{bmatrix} i_d^{+*} \\ i_q^{+*} \\ i_d^{-*} \\ i_q^{-*} \end{bmatrix} = \frac{2}{3} \begin{bmatrix} e_d^+ & e_q^+ \\ e_q^+ & -e_d^+ \\ -Ke_d^- & Ke_q^- \\ -Ke_q^- & -Ke_d^- \end{bmatrix} \begin{bmatrix} \frac{P_0^*}{D} \\ \frac{Q_0^*}{E} \end{bmatrix} \tag{3}$$

where $K = 0, \pm 1$. $D = (e_d^+)^2 + (e_q^+)^2 - K[(e_d^-)^2 + (e_q^-)^2]$, $E = (e_d^+)^2 + (e_q^+)^2 + K[(e_d^-)^2 + (e_q^-)^2]$.

By tracking the current references in (3), the control aims of

This article has been accepted for publication in a future issue of this journal, but has not been fully edited. Content may change prior to final publication. Citation information: DOI 10.1109/TSG.2017.2648879, IEEE Transactions on Smart Grid

injecting three-phase symmetrical currents under unbalanced voltage conditions (if $K = 0$), eliminating reactive power oscillations (if $K = -1$), and eliminating active power oscillations (if $K = 1$), can be accomplished. The equation (3) is suitable for the analysis under both balanced and unbalanced voltage conditions.

C. Fault Current Analysis

Based on the current references determined by (3), the amplitudes of positive- and negative-sequence injection currents can be calculated as

$$\begin{cases} \left|\mathbf{I}_{dq}^{+}\right| = \dfrac{2}{3}\left|\mathbf{E}_{dq}^{+}\right| \cdot \sqrt{\left(\dfrac{P_0^*}{D}\right)^2 + \left(\dfrac{Q_0^*}{E}\right)^2} \\ \left|\mathbf{I}_{dq}^{-}\right| = \dfrac{2}{3}\left|K\right| \cdot \left|\mathbf{E}_{dq}^{-}\right| \cdot \sqrt{\left(\dfrac{P_0^*}{D}\right)^2 + \left(\dfrac{Q_0^*}{E}\right)^2} \end{cases} \tag{4}$$

where $|\mathbf{I}_{dq}^{m}|=|i_d^{m*}+ji_q^{m*}|$, $|\mathbf{E}_{dq}^{m}|=|e_d^{m}+je_q^{m}|$, $(m=+,-)$.

The power reference signals in (4) are substituted with the actual apparent power provided by the PV unit during a fault and (4) can be rearranges as

$$\begin{cases} \left|\mathbf{I}_{dq}^{+}\right| = \dfrac{2}{3\gamma E_m}\sqrt{\left(\dfrac{P_0'}{1-K\beta^2}\right)^2 + \left(\dfrac{Q_0'}{1+K\beta^2}\right)^2} \\ \left|\mathbf{I}_{dq}^{-}\right| = \dfrac{2\beta}{3\gamma E_m}\left|K\right|\sqrt{\left(\dfrac{P_0'}{1-K\beta^2}\right)^2 + \left(\dfrac{Q_0'}{1+K\beta^2}\right)^2} \end{cases} \tag{5}$$

where γ is the coefficient of the positive-sequence voltage sag, K is the control factor, E_m is the pre-fault voltage amplitude at the point of common coupling (PCC), $\beta=|\mathbf{E}_{dq}^{-}|/|\mathbf{E}_{dq}^{+}|$ is a measure of the voltage unbalance, P_0' and Q_0' are the average values of the active and reactive powers supplied by the PV unit during a fault.

In a three-phase three-wire system, grid currents consist of the positive- and negative-sequence components

$$\begin{cases} I_a = \left|\mathbf{I}_{dq}^{+}\right|\cos(\omega t+\theta^+) + \left|\mathbf{I}_{dq}^{-}\right|\cos(\omega t-\theta^-) \\ I_b = \left|\mathbf{I}_{dq}^{+}\right|\cos(\omega t-2\pi/3+\theta^+) + \left|\mathbf{I}_{dq}^{-}\right|\cos(\omega t+2\pi/3-\theta^-) \\ I_c = \left|\mathbf{I}_{dq}^{+}\right|\cos(\omega t+2\pi/3+\theta^+) + \left|\mathbf{I}_{dq}^{-}\right|\cos(\omega t-2\pi/3-\theta^-) \end{cases} \tag{6}$$

where $\theta^+=\arctan(i_q^+/i_d^+)$ and $\theta^-=\arctan(i_q^-/i_d^-)$.

Substitute (5) into (6) and the three-phase instantaneous fault currents can be calculated as

$$\begin{cases} I_a = I_{am}\sin(\omega t+\varphi_a) \\ I_b = I_{bm}\sin(\omega t+\varphi_b) \\ I_c = I_{cm}\sin(\omega t+\varphi_c) \end{cases} \tag{7}$$

The amplitudes I_{am}, I_{bm}, and I_{cm} in (7) are detailed as

$$\begin{cases} I_{am} = \left|\mathbf{I}_{dq}^{+}\right|\sqrt{1+(K\beta)^2+2\left|K\right|\beta\cos\varphi} \\ I_{bm} = \left|\mathbf{I}_{dq}^{+}\right|\sqrt{1+(K\beta)^2+2\left|K\right|\beta\cos(-4\pi/3+\varphi)} \\ I_{cm} = \left|\mathbf{I}_{dq}^{+}\right|\sqrt{1+(K\beta)^2+2\left|K\right|\beta\cos(4\pi/3+\varphi)} \end{cases} \tag{8}$$

where $\varphi=\theta^++\theta^-=\arctan(e_q^-/e_d^-)$, is the phase shift of the negative-sequence voltage at the PCC.

The phases φ_a, φ_b and φ_c in (7) are detailed as (9). The analysis above implicates that the PV fault current is determined by several factors: γ, β, P_0' and Q_0'. The converter has fast dynamic response for current profile under the current control scheme, in which the fault transient can be almost ignored, as proved in [29]. The positive and negative sequences are controlled separately in the inner loops and the PV inverter can achieve stable positive and negative sequence impedances quickly once a fault occurs. The PV panel itself has no rotational inertia. Then the PV source can provide stable current shortly after the grid disturbance, and no current distortions appear in fault conditions, as described in (7). The PV panel's I-V characteristic can help restore the dc-link power balance [13], which makes the fault current enter into the steady state smoothly.

$$\begin{cases} \varphi_a = \arctan\dfrac{\cos\theta^+ + \left|K\right|\beta\cos\theta^-}{-\sin\theta^+ + \left|K\right|\beta\sin\theta^-} \\ \varphi_b = \arctan\dfrac{\cos(2\pi/3-\theta^+) + \left|K\right|\beta\cos(2\pi/3-\theta^-)}{\sin(2\pi/3-\theta^+) - \left|K\right|\beta\sin(2\pi/3-\theta^-)} \\ \varphi_a = \arctan\dfrac{\cos(2\pi/3+\theta^+) + \left|K\right|\beta\cos(2\pi/3+\theta^-)}{-\sin(2\pi/3+\theta^+) - \left|K\right|\beta\sin(2\pi/3+\theta^-)} \end{cases} \tag{9}$$

In PV power plants, static var generators (SVGs) are equipped to offset reactive power losses on the circuit elements and support the bus voltage during voltage sags. Thus PV units work at unity power factor during faults (Q_0' in (5) is zero). The control that allows the injection of symmetrical three-phase currents (K=0) can avoid current distortions and overcome the converter overcurrent effectively, which assists the FRT accomplishment. The disconnection of a large-scale PV power plant may jeopardize the system stability. Therefore, this control is used within the plant (In Section IV, the field-testing data can confirm this). The post-fault currents in (7) are further simplified as

$$\begin{cases} I_a = \dfrac{2P_0'}{3\gamma E_m}\sin(\omega t+\dfrac{\pi}{2}+\theta^+) \\ I_b = \dfrac{2P_0'}{3\gamma E_m}\sin(\omega t-\dfrac{\pi}{6}+\theta^+) \\ I_c = \dfrac{2P_0'}{3\gamma E_m}\sin(\omega t+\dfrac{7\pi}{6}+\theta^+) \end{cases} \tag{10}$$

With the control (K=0), the post-fault currents from the inverter are symmetrical during both balanced and unbalanced fault conditions and the amplitude is determined by factors P_0' and γ. The active power P_0' is dependent on the output power from the PV array during the fault and the PV array output is determined by the operating point on the I-V characteristic curve of the PV panel [30].

Normally the PV array operates at or around the maximum power point (MPP). However, voltage disturbances can cause the PV array to deviate away from the MPP and reduce the output power. For a balanced fault, the dc-link voltage will increase and the PV array operates away from the MPP. For an unbalanced fault, the active power from the PV inverter is superimposed with a second harmonic oscillation. This oscillation will induce dc-link voltage fluctuations and cause the PV array operation to deviate from the MPP as well. The PV output power reduction is related to the fault severity. Considering the PV panel's special characteristic and the factor γ dependent on the fault position and type, it is hard to quantitate the relationship between P_0' and the fault severity and impossible to perform precise calculation of PV fault currents.

Although the PV panel's special *I-V* characteristic makes the accurate calculation of the fault currents difficult, it helps reduce the fault currents and enhance the FRT ability. This feature can quickly balance the power difference at dc side in fault conditions, which results in short transients at ac side and almost no harmonic and attenuation components. The abovementioned fault current analysis indicates that it is hard to establish an accurate PV fault calculation expression. Therefore, the conventional current protection that relies on fault current setting calculations is unable to apply. However, the PV fault current characteristics provide potential applications for the distance relay based on the system frequency measurement.

III. Evaluation on Protection Within the Collection System

Based on the fault current analysis in Section II, the performance of the existing current protection is evaluated in Section III and some deficiencies are revealed. Then a distance protection scheme is proposed to effectively isolate PV side from faults on overhead lines.

A. Existing Protection Scheme

The existing protection scheme of the collection lines within the PV power plant are as follows: 1) overcurrent and zero-sequence current relays are equipped on the cable; 2) pilot current, overcurrent and zero-sequence current relays are equipped on the overhead line.

B. Performance of the Overcurrent Relays

The coordination principles of the OCRs are detailed in Table I. The performance of the existing OCRs is evaluated considering the fault analysis in Section II.

For a fault on one cable, as f_1 in Fig. 3, the relay measured current is supplied by the grid, the neighboring overhead lines and cables. This current is large enough to trigger the OCR on the cable due to the grid-side large short-circuit capacity. Similarly, the OCR on the overhead line, which links the faulted cable, can initiate its zone II and III protection. The downstream OCR's zone I has a sensitivity higher than 2 (covers a longer distance) in case of a three-phase fault at the end of the protected line. This might cause the downstream OCR on the overhead line in malfunction when a close-end fault occurs.

For a fault on one overhead line, as f_2 in Fig. 3, the fault current from the upstream side is supplied by the grid and the adjacent overhead lines and then the upstream OCR can operate correctly due to the grid-side large short-circuit current. On the opposite side of the overhead line, the fault current from the downstream side is contributed by the linked PV units. The OCRs on the overhead lines have the setting values higher than the maximum fault current supplied by the PV inverters (1.1-1.2 times the rated current in commercial products). Thus the OCRs on the neighboring lines are prevented from malfunction. However, the downstream OCR of the faulted overhead line cannot operate due to the limited fault current. When the pilot relay is out of service, the downstream OCR cannot operate and the fault cannot be isolated from the PV units either. This results in the PV units contributing currents to the point of failure, which may damage the circuit elements and bring risk to the maintenance personnel.

In summary, the existing OCR at downstream side on the overhead line has two problems: 1) mal-operation in case of a fault close to the breaker on the cable; 2) mis-operation in case of a fault on the overhead line.

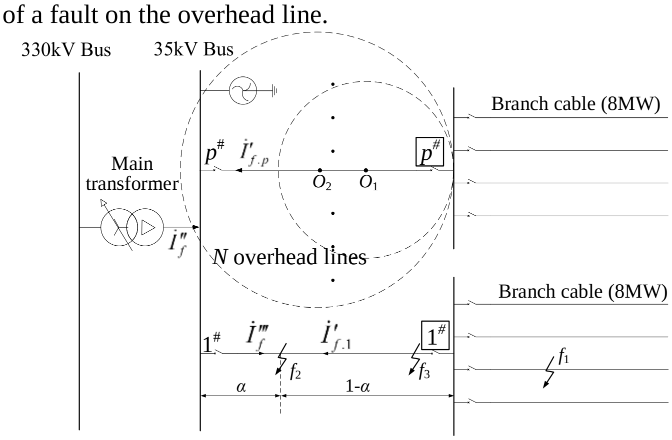

Fig. 3. Schematic diagram of the collection system.

TABLE I Coordination principles of the OCRs in the collection system

Location	Protection		Coordination Principle	Setting Value	Delay
Overhead line (Upstream, System side)	OCR	Zone I	Sensitivity of 2 in case of a fault at the end	$0.866I_{f(3)}/2$	0.1s
		Zone II	Coordination with next zone I	$1.2\times 6I_e$	0.6s
		Zone III	Maximum load current	$1.3nI_e$	0.9s
Overhead line (Downstream, PV side)	OCR	Zone I	Coordination with upstream zone I	$(0.866I_{f(3)}/2)/1.1$	0s
		Zone II	Coordination with next zone I	$1.2\times 6I_e$	0.3s
		Zone III	Maximum load current	$1.3nI_e$	0.6s
Cable	OCR	Zone I	Step-up transformer inrush current	$6I_e$	0s
		Zone II	Maximum load current	$1.3I_e$	0.3s

$I_{f(3)}$ means the short-circuit current from the upstream in case of a three-phase fault at the overhead line end.
I_e is the rated current supplied by PV units on one cable.
n means the number of cables linked with one overhead line.

C. Proposed Protection Scheme

When the fault position is close to the upstream side on the overhead line, the faulted overhead line and the neighboring overhead lines share the similar voltage profile and then it is difficult to distinguish the fault current from the PV side on the faulted overhead line from those on the adjacent overhead lines. In addition, the currents through the downstream relay on the faulted and non-fault overhead lines have the identical direction. Hence it is impossible to pick out the faulted section using just the current information at the local relay measurement.

The communication based protection cannot avoid the reliability problem (in case of communication failure), so that the local information based solution is preferred. The analysis in Section II indicates that the PV unit provides the stable fundamental-frequency fault current, and based on that a two-zone directional distance relay (shown as the dashed circles in Fig. 3) is proposed to replace the OCR at the downstream side on the overhead line.

The 35 kV side of the main transformer connects N overhead lines. For a fault such as f_2 on overhead line $1^{\#}$, as shown in Fig. 3, the fault current from the PV side on overhead line $i^{\#}$ is denoted by $\dot{I}'_{f.i}$ (i=1, …, N), and the short-circuit current from the grid side is denoted by $\dot{I}''_f$.

The current flowing to the point of failure via the upstream relay location can be expressed as

$$\dot{I}'''_f = \dot{I}''_f + \sum_{i=2}^{N} \dot{I}'_{f.i} \tag{11}$$

The measured voltage at the downstream relay $p^{\#}$ can be obtained with the line impedance and the fault current through the relay

$$\dot{U}_{m.p} = \dot{I}'_{f.p} Z_1 + \dot{I}'''_f \alpha Z_1 = \dot{I}'_{f.p} Z_1 + [\sum_{i=2}^{N} \dot{I}'_{f.i} + \dot{I}''_f] \alpha Z_1 \tag{12}$$

where α is the ratio of the distance between the fault position and the relay location to the whole overhead line ($0<\alpha<1$), and Z_1 is the positive-sequence impedance of the overhead line.

Considering that the neighboring non-fault lines can see the same voltage distribution, the PV units on those lines have identical fault behaviors as: $\dot{I}'_{f.2}=\dot{I}'_{f.3}=\cdots=\dot{I}'_{f.N}$.

The measured impedance at relay $p^{\#}$ can be calculated with the measured current $\dot{I}_{m.p}=\dot{I}'_{f.p}$

$$Z_{m.p} = \frac{\dot{U}_{m.p}}{\dot{I}_{m.p}} = Z_1[1+\alpha(n-1)+\alpha\frac{\dot{I}''_f}{\dot{I}'_{f.p}}] \tag{13}$$

where N=7 within this plant, and then $Z_{m.p}=Z_1[1+\alpha(6+\dot{I}''_f/\dot{I}'_{f.p})]$. Because the grid capacity is much greater than the rated PV capacity on one overhead line, $|\dot{I}''_f/\dot{I}'_{f.p}|$ is a large value. The value of $|\dot{I}''_f/\dot{I}'_{f.p}|$ will become larger in case of the PV output power at a lower level. Influenced by the grid-side short-circuit current, the measured impedance at relay $p^{\#}$ is much larger than the actual impedance between the relay installation and the fault position. Therefore, it can be used to discriminate the faulted overhead line from the non-fault ones.

In consideration of an extremely serious situation that the fault is almost at the upstream relay on the overhead line (α=0), the measured impedance at the downstream relays will be the respective line impedances. If the distance relay is set with only one zone, in order to prevent the neighboring lines from mal-operation, zone I should not operate until the opposite OCR operate and isolate the neighboring overhead lines from the fault. This leads to the distance relays operating with a time delay (>0.9 s, as the real system's relay settings shown in Table I) wherever the fault occurs on the overhead line.

In order to isolate the PV side from the fault as soon as possible, zone II with a time delay is coordinated with zone I. Zone I covers part of the overhead line, in which the fault can be isolated without delay, whereas zone II covers the whole line and has a time delay longer than the upstream OCR's to deal with the extremely serious situation (α=0). For faults on the cable, it is seen by the directional distance relay as outside the operation region. At this moment, the upstream OCR on the overhead line coordinates with that on the cable and this can ensure the correct relay operation.

Considering the appropriate margin, the detailed principle of the proposed distance relay is set as

$$\begin{cases} Z_{set}^{\mathrm{I}} = K_{rel.\mathrm{I}} Z_1 \quad (K_{rel.\mathrm{I}}=85\%) \;\; \Delta t_{\mathrm{I}} = 0s \\ Z_{set}^{\mathrm{II}} = K_{rel.\mathrm{II}} Z_1 \quad (K_{rel.\mathrm{II}}=1.2) \;\; \Delta t_{\mathrm{II}} > 0.9s \end{cases} \tag{14}$$

where K_{rel} is the reliability factor.

IV. Field-Testing and Simulation Results

A. Comparison Between Field-Testing and Simulation Results

A real short-circuit test was carried out within the plant, and the fault was imposed on one overhead line near to the downstream relay (α is close to 1), marked as f_3 in Fig. 3. The network and line parameters of the collection system in Fig. 1 are listed in Table A.I and Table A.II of Appendix. The cable length between two PV units ranges from 0.14 km to 0.17 km, and that between the 35 kV bus and the first PV unit ranges from 0.17 km to 0.43 km.

The voltage on the upstream bus of the faulted overhead line is shown in Fig. 4(a). The fault applied at 8.86 s was phase B to ground (BG), then changed into phases B and C to ground (BCG) at 9.09 s. At 9.17 s, the faulted overhead line was isolated by the relay operation. Before the artificial test, the PV units output about 0.6 pu the rated power and worked at unity power factor. The step-up transformers (35/0.3 kV) have Y/d connections and the main transformer (330/35 kV) has YN/d connections. The grounding transformer was not working during the test (In normal operation, the ground transformer is in service all the time.), so the secondary side of the step-up transformers did not experience any significant increase in the current during the period of single line to ground (SLG), as shown in Fig. 4(b). The currents in Fig. 4(b) were recorded by the measurement at the upstream relay on a neighboring overhead line and they were supplied only by the PV units.

As shown in the Fig. 4(b), during the period of BCG fault (9.09 s-9.17 s), the fault currents from the PV side keep symmetrical and have no obvious attenuation and harmonic components. In case that the fault current amplitude does not reach the upper limit (1.1-1.2 pu in commercial products), the fault current increase is not in proportion to the voltage sag

This article has been accepted for publication in a future issue of this journal, but has not been fully edited. Content may change prior to final publication. Citation information: DOI 10.1109/TSG.2017.2648879, IEEE Transactions on Smart Grid

degree. This is related to the reduction of output power from the PV arrays which operated away from their MPP during the fault. With the voltages and currents of the above measurement, the active and reactive powers from the PV side are calculated as shown in Fig. 5.

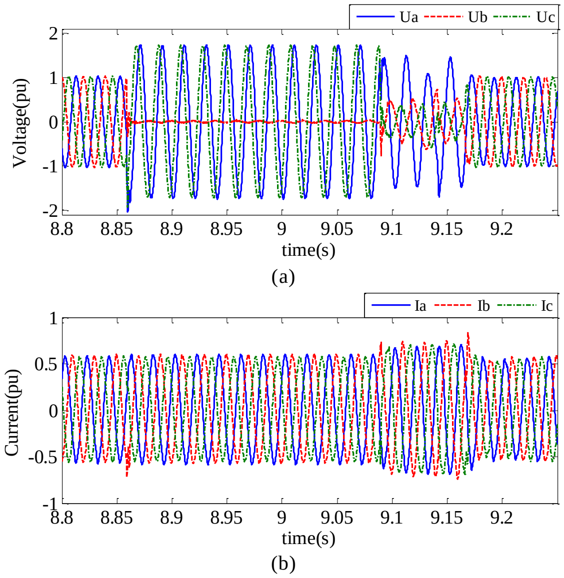

Fig. 4. Voltages and currents recorded during the short-circuit test. (a) Voltages on 35kV bus. (b) Currents through the upstream relay on the neighboring overhead line.

In the duration of BCG, the dc component P_0 of the active power experiences an obvious decrease. The conventional fault analysis regards that PV sources can provide a constant power after a fault, which is not suitable for a centralized PV power plant. The field-testing results show that under unbalanced the fault, the fault currents from PV side keep symmetrical and have short transients. The fault current amplitude is affected by the PV panel's *I-V* characteristic. The field-testing results verified the analysis on fault currents contributed by the PV unit as described in Section II.

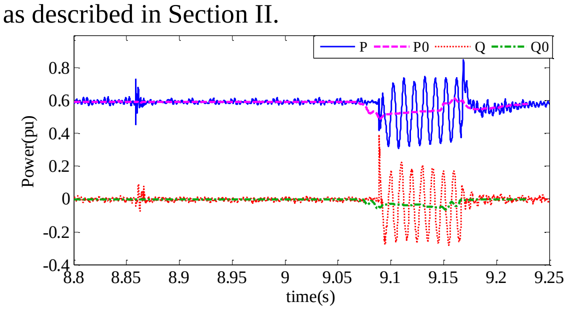

Fig. 5. Instantaneous power flow at the measuring point.

In PSCAD/EMTDC, a detailed model of the collection system in Fig. 1 was built with the same control. The PV inverter model parameters are given in Table A.III of Appendix, instead of those in the real inverter which is packaged for commercial confidentiality. The above field-testing scenario was reproduced in the model and the simulation results are shown in Fig. 6.

Compared with the field-testing results in Fig. 4, the PV model produces highly similar fault current characteristics. The fault transient in Fig. 6(b) experiences a little longer time for about 20 ms, which is mainly caused by notch filters rather than the current controllers. It is hard to fully duplicating the real inverter control performance for the unknown parameters inside of a commercial inverter. The relatively small transient differences in the simulations are acceptable. The transient will make the measured impedance at PV side unstable slightly. In order to ensure the reliability of the proposed protection, the distance element uses the stable information to determine the impedance. This slight delay has no significant effect on protection coordination.

In order to demonstrate the influence of the PV panel, for a line-to-line (CA) fault, the output characteristics of the PV array are shown in Fig. 7. The dc-link voltage $U(t)$, the output power $P(t)$ against time and the PV array's operating point on its *P-U* curve are plotted. These all fluctuate at a double system frequency, which are consistent with the analysis in Section II. The fluctuation of the dc-link voltage $U(t)$ makes the PV array operate from the MPP and leads to an obvious decrease in the output power. This can help reduce the fault current but makes the fault current estimation challenging.

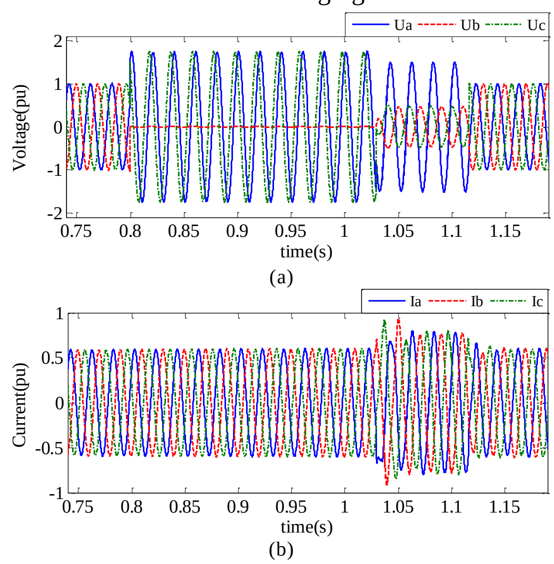

Fig. 6. Voltage and current waveforms of simulation results. (a) Voltages on the 35kV bus. (b) Currents through the upstream relay on the neighboring overhead line.

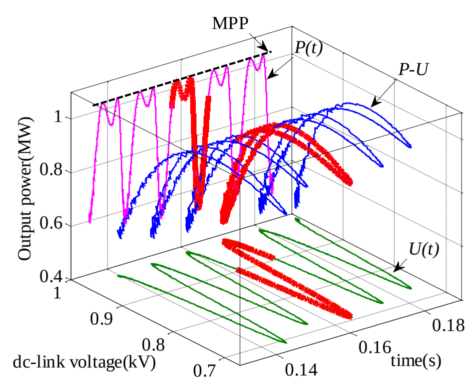

Fig. 7 Output characteristics of the PV array in case a CA fault at grid side.

B. Fault Characteristic under Variant Controls

The equation (3) is obtained from three typical control cases (K=0, ±1). In practice, the control scheme used may not be limited to those and the factor K may be varying to make a tradeoff between the fault current amplitude and the power oscillations. The simulation results with K increasing smoothly are illustrated in Fig. 8. The fault is employed between phases A and B, and the power references are P_0^*=0.5 MW, Q_0^*=0.5 MVar.

During the period of 0.1 s-0.2 s, K is increasing evenly from -1 to +1. As Fig. 8(b) shows, the active power oscillation decreases gradually to zero, meanwhile an oscillation in the reactive power grows and eventually up to the initial level of the active power. The grid current is not distorted during the dynamic tuning of K. The changes in the fault current are only the amplitudes of each phase. The proposed protection at the PV side is based on system frequency measurement. As shown in Fig. 8(c), the grid current with K varying experiences no frequency deviation and then the proposed protection has no phasor extraction problem. Therefore, the proposed protection is not affected by the coefficient variation and generally suitable for flexible control schemes.

PV power plants should have the capability of offsetting reactive power losses and supporting the grid voltage when the grid voltage experiences sags. In Fig. 8, the inverter works with the reactive power supplying to meet the voltage support requirement. The grid currents do not experience any current distortion with the variant value of K. Therefore, the proposed protection design is immune to the voltage support requirement for the inverters.

Specially, when K is equal to zero, the minimum fault current appears. Meanwhile, the active and reactive powers share the power oscillations equally, which have the minimum amplitude. Due to this performance, the control scheme with K=0 is used in those on-site inverters, as proved in Fig. 4 and Fig. 5. The situation is a typical case where the proposed protection is applied in next section but not limited to this application.

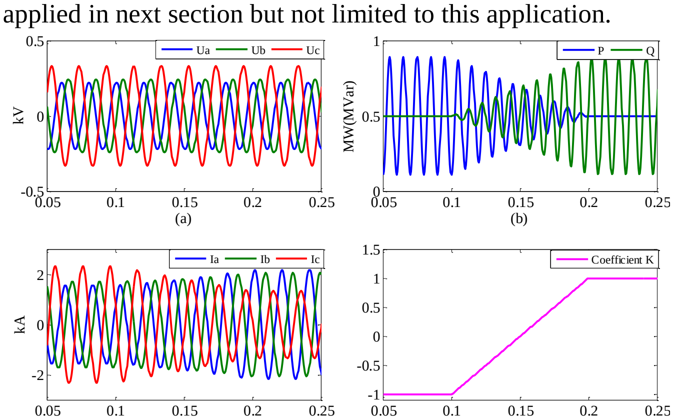

Fig. 8 Simulation results of the flexible control with -1<K<+1. (a) Grid voltage. (b) Inverter output powers. (c) Grid current. (d) The factor K.

C. Verification of the Proposed Protection Scheme

It has been confirmed that the simulation PV model has consistent fault current characteristics with those within the plant. The simulation model is used to comprehensively evaluate the performance of the existing OCR design and the proposed distance relay design.

The PV units operated at 0.6 pu the rated power and a BC fault occurred at midpoint on one overhead line. As shown in Fig. 9, the PV fault current on the faulted line is about 1 pu and that on the neighboring line is about 0.8 pu. The fault currents cannot even reach zone II and III of the downstream OCR, whose zone I has a higher setting value and is not plotted in Fig. 9. The downstream OCRs on both the faulted and neighboring overhead lines cannot operate and then the PV units continue to contribute fault currents to the faulted point.

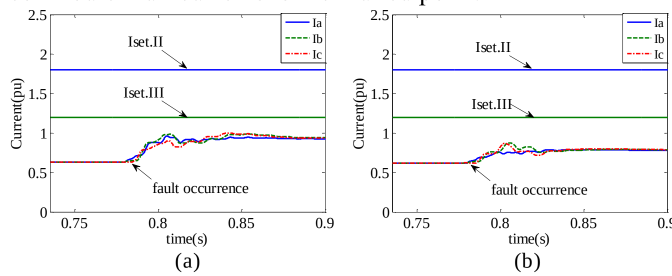

Fig. 9. OCRs operation results at downstream side on the overhead lines in case a BC fault at midpoint of one overhead line. (a) Results of the OCR operation on the faulted overhead line. (b) Results of the OCR operation on the neighboring overhead line.

In order to verify the proposed distance relay at PV side, all the factors that includes the system capacity, the PV output level and fault types, are considered in the simulations. Here gives two typical cases:

Case 1

When the ratio of the PV power plant's rating capacity to the external grid's is 1:10 and the plant works at 0.6 pu, an ABG fault occurs on the overhead line 10% l away from the downstream relay location (l is the line length). The protection zones of the ground distance relay and the phase distance relay are depicted in Fig. 10(a) and Fig. 10(b), respectively. The similar results from the neighboring line are shown in Fig. 10(c) and Fig. 10(d). The measured impedances of the ground distance elements (AG and BG) and the phase distance element (AB) on the faulted overhead line fall in zone I constantly, as shown in Fig. 10(a) and Fig. 10(b). The measured impedances of the distance elements on the neighboring overhead line all fall outside the protection zones as shown in Fig. 10(c) and Fig. 10(d). Therefore, AG, BG and AB distance elements on the faulted overhead line can operate correctly.

This article has been accepted for publication in a future issue of this journal, but has not been fully edited. Content may change prior to final publication. Citation information: DOI 10.1109/TSG.2017.2648879, IEEE Transactions on Smart Grid

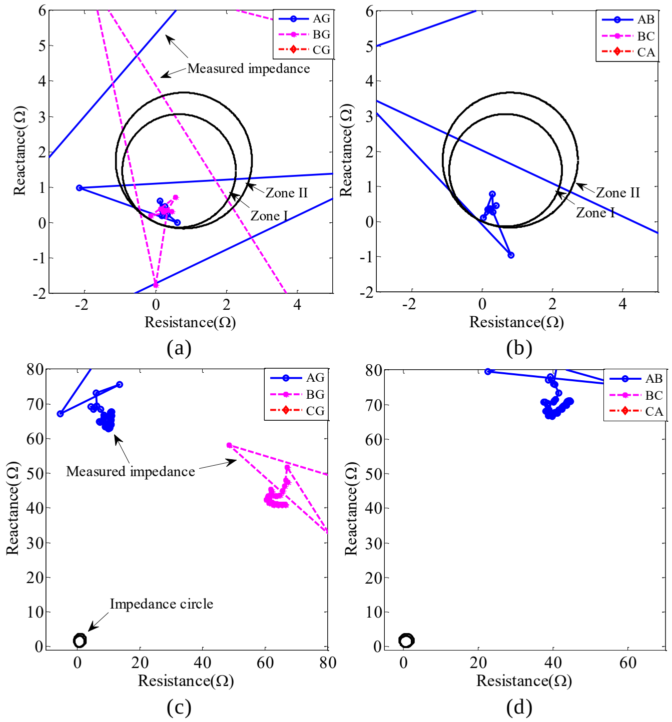

Fig. 10 Operation results of the distance relays at downstream side on the overhead lines in case of an ABG fault 10% *l* away from the downstream relay location. (a) (c) The ground distance relay operation results on the faulted and neighboring overhead lines, respectively. (b) (d) The phase distance relay operation results on the faulted and neighboring overhead lines, respectively.

Case 2

When the ratio of the PV power plant's rating capacity to the external grid's becomes 1:30 and the plant increases the output power to 0.8 pu, a CA fault occurs on one overhead line 90% *l* from the downstream relay location. As shown in Fig. 11, only the measured impedance of the phase distance element (CA) on the faulted overhead line falls in zone II whereas the distance relay on the neighboring overhead line cannot operate.

In practice, the relay with the quadrangle characteristic should be used to enhance the relay performance to the fault resistance. Faults on the cable are regarded as external faults by the directional element and this guarantees no mal-operation.

In Table II, the performances of the existing and the proposed relays are presented when different fault positions, fault types and output levels of the PV power plant are considered. In the table, the symbol + (-) represents the protection can (not) operate and the Roman number represents the corresponding operation zone. For faults near the relay installation on the cable, the directional distance element detects the faults outside the protection zone whereas the OCR at downstream side on the faulted overhead line can operate. For faults on the overhead line, the distance relay responses correctly to the fault positions and isolates the fault whereas the OCR cannot. The proposed distance relay can operate correctly in case of different fault positions, PV output levels and fault types. In case the pilot relay is out of service, the distance relay can isolate the PV system from the fault correctly. The SLG faults within the plant are not included in Table II, because fault currents from the PV side do not experience significant increase and the OCRs do not operate (as shown in Fig. 9). However, the distance relay still has a good performance due to the correct impedance estimation.

Affected by the variant control strategies, the PV inverter impedance is unregulated and the positive sequence may be not equal to the negative sequence any more. The distance protections based on the known PV source impedance, such as the fault component based method, are not suitable for the application at PV side. However, the proposed protection scheme is not affected by the irregular PV impedance.

Since the external grid has a larger capacity than the PV capacity on one overhead line, the high-value fault resistance can increase the measured impedance at PV side. This may lead the relay to operating failure. The challenges caused by the high-value fault resistance are our future work.

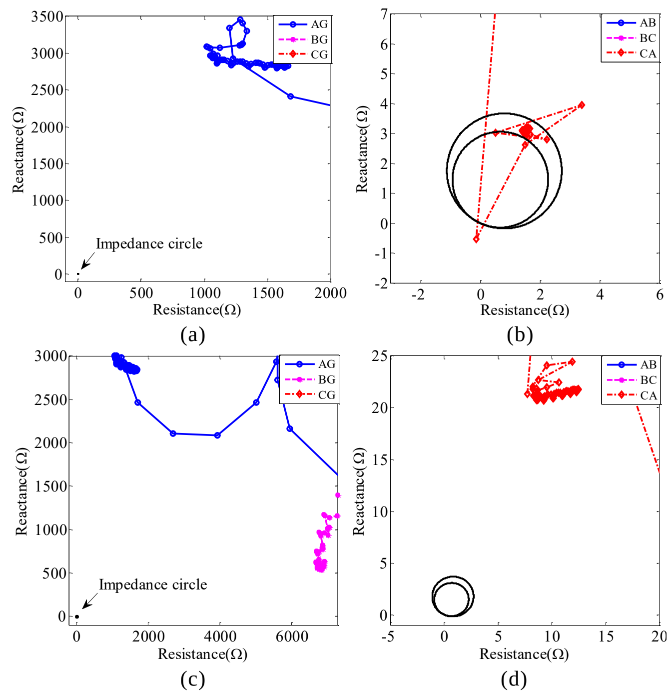

Fig. 11 Operation results of the distance relays at downstream side on the overhead lines in case of a CA fault 90% *l* away from the downstream relay location. (a) (c) The ground distance relay operation results on the faulted and neighboring overhead lines, respectively. (b) (d) The phase distance relay operation results on the faulted and neighboring overhead lines, respectively.

V. CONCLUSION

The fault current characteristics within a large PV power plant are analyzed considering the control used in practice. Both the field-testing and the simulation results show that the PV panel characteristic can help reduce the fault current, which challenges the conventional method of fault analysis and the existing coordination of OCRs. By comparing the field-testing results with the simulation results, the existing OCR are proved to have the problems of mis-operation and mal-operation. A distance relay based protection design is proposed to substitute for the defective OCR scheme. Simulation results show that the proposed relay can effectively solve the existing OCR's problems. Apart from being highly robust to variant fault scenarios, the proposed protection has a good performance in case of different output levels of the PV power plant and so can meet the requirements for industrial applications.

TABLE II Operation results of the original and the proposed relays

Fault locations		PV output levels	Fault types	Overcurrent relays			Distance relay
				Cable	Overhead line		
					Downstream	Upstream	Downstream
Cable	Close to the relay location	40%	LL	+	+	**II, III**	-
			LLG	+	+	**II, III**	-
			LLL	+	+	**II, III**	-
		80%	LL	+	+	**II, III**	-
			LLG	+	+	**II, III**	-
			LLL	+	+	**II, III**	-
Overhead line	α=0.5	20%	LL	-	-	+	+
			LLG	-	-	+	+
			LLL	-	-	+	+
		60%	LL	-	-	+	+
			LLG	-	-	+	+
			LLL	-	-	+	+
	α=0.9	60%	LL	-	-	+	**II**
			LLG	-	-	+	**II**
			LLL	-	-	+	**II**
		100%	LL	-	-	+	**II**
			LLG	-	-	+	**II**
			LLL	-	-	+	**II**

APPENDIX

TABLE A.I Network parameters of the collection system

Line	Line type	Line length (km)
Overhead line #1	1	8.34
Overhead line #2	1	8.35
35kV Bus-PV #1	2	0.17~0.43
PV #1-#2	2	0.14~0.17
PV #2-#8	3	(0.14~0.17)×6

TABLE A.II Line parameters of the collection system

Line type	Resistance per unit length (Ω/km)	Resistance per unit length (Ω/km)
1	0.175	0.380
2	0.26	0.132
3	0.37	0.132

TABLE A.III PV inverter parameters

Parameters	Description	Value
P_N	PV inverter rating	500 kW
L_i	Inverter-side filter inductance	0.2 mH
L_g	Grid-side filter inductance	0.2 mH
C_f	Filter capacitance	150 μF
f_{sw}	Switching frequency	3 kHz
f	Grid frequency	50 Hz
U_{dc}	DC-link voltage	750 V
K_p	Proportional gain factor	8.33
T_i	Integral time constant	2.5 ms

REFERENCES

[1] S. Kouro, J. I. Leon, D. Vinnikov, and L. G. Franquelo, "Grid-connected photovoltaic systems: An overview of recent research and emerging PV converter technology," *IEEE Ind. Electron. Mag.*, vol. 9, no. 1, pp. 47–61, Mar. 2015.

[2] M. Munsell, "GTM Research: Global Solar PV Installations Grew 34% in 2015, " Jan, 2016. [Online]. Available: http://www.pv-tech.org/news/global-solar-installations-hit-59gw-in-2015-gtm

[3] L. Ma, H. Liao, J. Li, X. Yang, K. Tschegodajew, and F. Tang, "Analysis of Chinese photovoltaic generation system low voltage ride through characters," in *Proc. IEEE 7th Int. Power Electron. Motion Control Conf.*, Jun. 2012, pp. 1178–1182

[4] E. Troester, "New German grid codes for connecting PV systems to the medium voltage power grid," in *Proc. 2nd Int. Workshop Concentrating Photovoltaic Power Plants: Opt. Design, Prod., Grid Connection*, 2009, pp. 1–4.

[5] H.-S. Song and K. Nam, "Dual current control scheme for PWM converterunder unbalanced input voltage conditions," IEEE Trans. Ind. Electron.,vol. 46, no. 5, pp. 953–959, Oct. 1999.

[6] M. Mirhosseini, J. Pou, B. Karanayil, and V. G. Agelidis, "Positive- and negative-sequence control of grid-connected photovoltaic systems under unbalanced voltage conditions," in *Proc. Australasian Univ. Power Eng. Conf. (AUPEC)*, Sep. 2013, pp. 1–6.

[7] F. Wang, J. L. Duarte, and M. A. M. Hendrix, "Pliant active and reactive power control for grid-interactive converters under unbalanced voltage dips," *IEEE Trans. Power Electron.*, vol. 26, no. 5, pp. 1511–1521, May 2011.

[8] P. Rodriguez, A. V. Timbus, R. Teodorescu, M. Liserre, and F. Blaabjerg, "Flexible active power control of distributed power generation systems during grid faults," IEEE Trans. Ind. Electron., vol. 54, no. 5, pp. 2583–2592, Oct. 2007.

[9] X. Guo, W. Liu, X. Zhang, X. Sun, Z. Lu, and J. M. Guerrero, "Flexible control strategy for grid-connected inverter under unbalanced grid faults without PLL," *IEEE Trans. Power Electron*., vol. 30, no. 4, pp. 1773–1778, Apr. 2015.

[10] M. Castilla, J. Miret, J. Sosa, J. Matas, and L. G. de Vicuna, "Gridfault control scheme for three-phase photovoltaic inverters with adjustable power quality characteristics," *IEEE Trans. Power Electron.*, vol. 25, no. 12, pp. 2930–2940, Dec. 2010.

[11] J. Miret, M. Castilla, A. Camacho, L. Garcia de Vicuna, and J. Matas, "Control scheme for photovoltaic three-phase inverters to minimize peak currents during unbalanced grid-voltage sags," *IEEE Trans. Power Electron.*, vol. 27, no. 10, pp. 4262–4271, Oct. 2012.

[12] X. Guo, W. Liu, X. Zhang, and H. Geng, "Control strategy for microgrid inverter under unbalanced grid voltage conditions," in *IEEE 23rd Int. Symp. on Ind. Electron. (ISIE)*, 2014, pp. 2354-2358.

[13] M. Mirhosseini, J. Pou, andV.G.Agelidis, "Single- and two-stage inverterbased grid-connected photovoltaic power plants with ride-through capability under grid faults," *IEEE Trans. Sustainable Energy*, vol. 6, no. 3,pp. 1150–1159, Jul. 2015.

[14] J. Martinez and J. Martin-Arnedo, "Impact of distributed generation on distribution protection and power quality," in *Proc. IEEE Power Energy Society General Meeting, PES'09*, Jul. 2009, pp. 1–6.

[15] F. Abu-Mouti and M. El-Hawary, "Optimal distributed generation allocation and sizing in distribution systems via artificial bee colony algorithm," *IEEE Trans. Power Del.*, vol. 26, no. 4, pp. 2090–2101, Oct. 2011.

This article has been accepted for publication in a future issue of this journal, but has not been fully edited. Content may change prior to final publication. Citation information: DOI 10.1109/TSG.2017.2648879, IEEE Transactions on Smart Grid

[16] R. Shayani and M. de Oliveira, “Photovoltaic generation penetration limits in radial distribution systems,” *IEEE Trans. Power Syst.*, vol. 26, no. 3, pp. 1625–1631, Aug. 2011.

[17] I. Xyngi and M. Popov, “An intelligent algorithm for the protection of smart power systems,” *IEEE Trans. Smart Grid*, vol. 4, no. 3, pp. 1541–1548, Sep. 2013.

[18] P. Mahat, Z. Chen, B. Bak-Jensen, and C. L. Bak, “A simple adaptive overcurrent protection of distribution systems with distributed generation,” *IEEE Trans. Smart Grid*, vol. 2, no. 3, pp. 428–437, Sep. 2011.

[19] M. Dewadasa, A. Ghosh, and G. Ledwich, “Protection of distributed generation connected networks with coordination of overcurrent relays,” in *Proc. 37th Annu. Conf. IEEE Ind. Elect. Soc. (IECON)*, Melbourne, VIC, Australia, 2011, pp. 924–929.

[20] J. Ma, X. Wang, Y. Zhang, Q. Yang, and A. G. Phadke, “A novel adaptive current protection scheme for distribution systems with distributed generation,” *Int. J. Elect. Power Energy Syst.*, vol. 43, no. 1, pp. 1460–1466, 2012.

[21] N. El Halabi, M. Garc ́a-Gracia, J. Borroy, and J. L. Villa, “Current phase comparison pilot scheme for distributed generation networks protection,” *Appl. Energy*, vol. 88, no. 12, pp. 4563–4569, 2011.

[22] D. S. Kumar, D. Srinivasan, T. Reindl, “A Fast and Scalable Protection Scheme for Distribution Networks With Distributed Generation.,” *IEEE Trans. on Power Del.*, vol. 31, no.1, pp. 67-75, 2016.

[23] A. Honrubia-Escribano, T. GarcíA-SáNchez, E. GóMez-LáZaro, et al. "Power quality surveys of photovoltaic power plants: characterisation and analysis of grid-code requirements," *IET Renew. Power Gener.*, vol. 9, no. 5, pp. 466-473, 2015.

[24] F. Liu, S. Duan, F. Liu, B. Liu, and Y. Kang, “A variable step size INC MPPT method for PV systems,” *IEEE Trans. Ind. Electron*., vol. 55, no. 7, pp. 2622–2628, Jul. 2008.

[25] P. Rodriguez, A. Luna, I. Candela, R. Rosas, R. Teodorescu, and F. Blaabjerg, “Multi-resonant frequency-locked loop for grid synchronization ofpower converters under distorted grid conditions,” *IEEE Trans. Ind. Electron*., vol. 58, no. 1, pp. 127–138, Jan. 2011.

[26] X. Guo, W. Wu, and Z. Chen, “Multiple-complex coefficient-filter-based phase-locked loop and synchronization technique for three-phase gridinterfaced converters in distributed utility networks,” *IEEE Trans. Ind*. Electron., vol. 58, no. 4, pp. 1194–1204, Apr. 2011.

[27] F. Freijedo, J. Doval-Gandoy, O. Lopez, and E. Acha, “Tunning of phase locked loops for power converters under distorted utility conditions,” in Proc. *24th Annu. IEEE Appl. Power Electron. Conf. (APEC) Exposition*, Feb. 2009, pp. 1733–1739.

[28] R. Kabiri, D. G. Holmes, B. P. McGrath, “Control of Active and Reactive Power Ripple to Mitigate Unbalanced Grid Voltages,” *IEEE Trans. Ind. Appl.*, vol. 52, no. 2, pp. 1660-1668, 2016.

[29] M. E. Baran and I. El-Markaby, “Fault analysis on distribution feeders with distributed generators,” *IEEE Trans. Power Syst.*, vol. 20, no. 4, pp. 1757–1764, Nov. 2005.

[30] J. J. Soon and K.-S. Low, “Optimizing photovoltaic model parameters for simulation,” in *Proc. IEEE Int. Symp. Ind. Electron*., 2012, pp. 1813–1818.